β decays of isotones with neutron magic number of $N = 126$ and r-process nucleosynthesis

Toshio Suzuki,[1,2,3] Takashi Yoshida,[4] Toshitaka Kajino,[3,4] and Takaharu Otsuka[5,6]

[1]*Department of Physics, College of Humanities and Sciences, Nihon University, Sakurajosui 3-25-40, Setagaya-ku, Tokyo 156-8550, Japan*
[2]*Center for Nuclear Study, University of Tokyo, Hirosawa, Wako-shi, Saitama 351-0198, Japan*
[3]*National Astronomical Observatory of Japan, Mitaka, Tokyo 181-8588, Japan*
[4]*Department of Astronomy, Graduate School of Science, University of Tokyo, Bunkyo-ku, Tokyo 113-0033, Japan*
[5]*Department of Physics and Center for Nuclear Study, University of Tokyo, Hongo, Bunkyo-ku, Tokyo 113-0033, Japan*
[6]*National Superconducting Cyclotron Laboratory, Michigan State University, East Lansing, Michigan 48824, USA*

β decays of the isotones with $N = 126$ are studied by shell-model calculations taking into account both the Gamow-Teller (GT) and first-forbidden (FF) transitions. The FF transitions are found to be important to reduce the half-lives, by nearly twice to several times, from those by the GT contributions only. Possible implications of the short half-lives of the waiting point nuclei on the r-process nucleosynthesis during the supernova explosions are discussed. A slight shift of the third peak of the element abundances in the r process toward a higher mass region is found.

I. INTRODUCTION

The r process is the most promising process for the synthesis of about half of heavy elements beyond iron [1]. Study of the r-process element synthesis has been done by considering neutrino-driven winds in supernova explosions [2] as well as ONeMg supernovae [3] and neutron-star mergers [4]. The production of the r-process elements in collapsars relating to long γ-ray bursts has also been investigated [5]. Recent observations of r-process elements in extremely metal-poor stars [6] have suggested that the r process has occurred in explosions of massive stars or in neutron-star mergers from the early stage of galactic chemical evolution. The r process is affected by various inputs of nuclear properties such as mass formulas [7], β-decay rates, (n, γ) and (γ, n) reaction cross sections, reaction rates of α processes in light nuclei [8], etc., and depends also on astrophysical conditions; electron-to-baryon number ratio, Y_e, the entropy and temperature of the explosion environment, and neutrino processes [9,10]. The evaluation of β-decay rates, particularly at the waiting point nuclei, is one of the important issues of the nucleosynthesis through the r process. Investigations on the β decays of isotones with neutron magic number of $N = 82$ have been done by various methods including shell model [11], quasiparticle random-phase approximation (QRPA)/finite-range droplet model (FRDM) [12], QRPA/extended Thomas-Fermi plus Strutinsky integral (ETFSI) [13], and Hartree-Fock-Bogoliubov (HFB) + QRPA [14] calculations as well as continuum quasiparticle random-phase approximation (CQRPA) ones [15]. The half-lives of nuclei obtained by these calculations are rather consistent to one another, and especially in shell-model calculations experimental half-lives at proton number of $Z = 47$, 48, and 49 are well reproduced [11].

For the β decays at $N = 126$ isotones, however, half-lives obtained by various calculations differ from one another [10]. First-forbidden (FF) transitions become important for these nuclei in addition to the Gamow-Teller (GT) transitions in contrast to the case of $N = 82$. A strong suppression of the half-lives for the $N = 126$ isotones due to the FF transitions has been predicted in Ref. [15]. Shell-model calculations of the β decays of $N = 126$ isotones have been done only with the contributions from the GT transitions [10,16]. Moreover, experimental data for the β decays in this region of nuclei are lacking. The region near the waiting point nuclei at $N = 126$ is therefore called the "blank spot" region.

Here, we study β decays of $N = 126$ isotones by taking into account both the GT and FF transitions to evaluate their half-lives. Shell-model calculations are done with the use of shell-model interactions, modified G-matrix elements, that reproduce well the observed energy levels of the isotones with a few (two to five) proton holes outside ^{208}Pb [17,18]. In Sec. II, GT and FF transition strengths for the $N = 126$ isotones are evaluated, and half-lives of the β decays are obtained by taking into account both the transitions. The calculated half-lives of the waiting point nuclei in the r process become shorter by including the contributions from the FF transitions. In Sec. III, possible implications of these half-lives for the r-process nucleosynthesis are discussed. A summary is given in Sec. IV.

II. TRANSITION STRENGTHS AND HALF-LIVES OF THE $N = 126$ ISOTONES

A. Gamow-Teller, spin-dipole transition strengths, and shape factors

First, the method for the evaluation of the rates and half-lives of the GT and FF transitions are explained. Then isotone dependence of the GT and FF transition strengths as well as the effects of the inclusion of the FF transitions on the half-lives of the isotones are discussed.

The decay rates Λ as well as the partial half-lives $t_{1/2}$ of the transitions are obtained by the following

formulas [19–21]:

$$\Lambda = \ln 2 / t_{1/2} = f/8896 \quad (\text{s}^{-1}),$$

$$f = \int_1^{w_0} C(w) F(Z, w) p w (w_0 - w)^2 dw, \qquad (1)$$

$$C(w) = K_0 + K_1 w + K_{-1}/w + K_2 w^2,$$

where w is the electron energy, $F(Z, w)$ is the Fermi function, and K_n's depend on nuclear transition-matrix elements. Here, relativistic corrections from the expansion of electron radial wave functions in powers of electron mass and nuclear charge parameters are included; matrix elements of one-body operators, $[\vec{r} \times \vec{\sigma}]^\lambda$ with $\lambda = 0, 1, 2$ and $\vec{r}$, as well as those from weak hadronic currents, γ_5, $\vec{\alpha}$, are taken into account for the FF transitions. In the case of the GT transition, the shape factor $C(w)$ does not depend on electron energy;

$$K_0 = \frac{1}{2J_i + 1} |\langle f || O(1^+) || i \rangle|^2, \quad O(1^+) = g_A \vec{\sigma} t_- \quad (2)$$

with g_A the axial vector coupling constant, J_i is the spin of the initial state, and $t_- |n\rangle = |p\rangle$, and $K_n (n \neq 0) = 0$.

In the case of the FF transitions, for 0^- transitions,

$$K_0 = \zeta_0^2 + \frac{1}{9}(M_0^S)^2, \quad K_{-1} = -\frac{2}{3}\mu_1 \gamma_1 \zeta_0 M_0^S,$$

$$\zeta_0 = V + \frac{1}{3}M_0^S w_0, \quad V = M_0^T + \xi M_0^{S'},$$

$$M_0^S = -g_A \sqrt{3} \langle f || ir[C_1 \times \vec{\sigma}]^0 t_- || i \rangle C, \qquad (3)$$

$$M_0^T = -g_A \langle f || \gamma_5 t_- || i \rangle C,$$

where $\xi = \alpha Z / 2R$ with α the fine-structure constant and R is the nuclear charge radius, $\gamma_1 = \sqrt{1 - (\alpha Z)^2}$, $C_L = \sqrt{4\pi/(2L + 1)} Y_L$, $C = 1/\sqrt{2J_i + 1}$. The prime in $M_0^{S'}$ indicates that the effects of the finite nuclear charge distribution on the electron wave function are taken into account [19,22]. For 1^- transitions,

$$K_0 = \zeta_1^2 + \frac{1}{9}(x + u)^2 - \frac{4}{9}\mu_1 \gamma_1 u(x + u)$$
$$+ \frac{1}{18}w_0^2(2x + u)^2 - \frac{1}{18}\lambda_2(2x - u)^2,$$

$$K_1 = -\frac{4}{3}uY - \frac{1}{9}w_0(4x^2 + 5u^2),$$

$$K_{-1} = \frac{2}{3}\mu_1 \gamma_1 \zeta_1(x + u),$$

$$K_2 = \frac{1}{18}[8u^2 + (2x + u)^2 + \lambda_2(2x - u)^2],$$

$$\zeta_1 = Y + \frac{1}{3}(u - x)w_0, \quad Y = \xi' y - \xi(u' + x'),$$

$$x = -\langle f || ir C_1 t_- || i \rangle C,$$

$$u = -g_A \sqrt{2} \langle f || ir[C_1 \times \vec{\sigma}]^1 t_- || i \rangle C,$$

$$\xi' y = -\langle f \left|\left| \frac{i}{M_N} \vec{\nabla} t_- \right|\right| i \rangle C,$$

where M_N is the nucleon mass and the primes in x' and u' indicate that the effects of finite nuclear charge distribution

are taken into account [19,22]. The quantities μ_1 and λ_2 are defined [20] in terms of electron wave functions and depend on electron momentum p_e. Their values are close to unity; $\mu_1 = 0.9$–1.0 and $\lambda_2 = 0.7$–1.0 at $p_e > 0.5$ and gets larger than 1 at $p_e < 0.5$ for Z considered here [23].

For 2^- transitions,

$$K_0 = \frac{1}{12}z^2(w_0^2 - \lambda_2), \quad K_1 = -\frac{1}{6}z^2 w_0,$$

$$K_2 = \frac{1}{12}z^2(1 + \lambda_2), \quad z = 2g_A \langle f || ir[C_1 \times \vec{\sigma}]^2 t_- || i \rangle C. \qquad (5)$$

In the leading order, the FF transition operators are expressed as [24]

$$C(w) = \frac{1}{2J_i + 1} |\langle f || O(\lambda^-) || i \rangle|^2,$$

$$O(0^-) = g_A \left[\frac{\vec{\sigma} \cdot \vec{p}}{M_N} + \xi i \vec{\sigma} \cdot \vec{r} \right] t_-,$$

$$O(1^-) = \left[g_V \frac{\vec{p}}{M_N} - \xi(g_A \vec{\sigma} \times \vec{r} - i g_V \vec{r}) \right] t_-, \qquad (6)$$

$$O(2^-)_\mu = i \frac{g_A}{\sqrt{3}} [\vec{\sigma} \times \vec{r}]_\mu^2 \sqrt{\vec{p}_e^2 + \vec{q}_v^2} t_-,$$

where g_V is the vector coupling constant. Matrix elements of the first and the second parts of $O(0^-)$, the first, second, and third terms of $O(1^-)$, and $O(2^-)$ correspond to M_0^T and $M_0^{S'}$, $\xi' y$, u', and x', and z in Ref. [19], respectively. The transition strengths constructed from the matrix elements of $O(0^-)$ and $O(1^-)$ in Eq. (6) are dominant parts of K_0, while that of $O(2^-)$ in Eq. (6) becomes equivalent to Eq. (5) when λ_2 equals unity.

A shell-model study was made for FF β decays in the lead region, $A = 205$–212, where an enhancement of the rank-zero matrix element of γ_5, M_0^T, has been found [25]. The quenching of the rank-1 and rank-2 components of the decay rate due to the core polarization effects has been also investigated [25,26]. Here, the transition-matrix elements and rates are evaluated by using Eqs. (1)–(5) following Refs. [19,20].

The isotones with proton number of $Z = 64$–73, that is, nuclei with $n_h = 18$–9 proton holes are considered here for the shell-model calculations [27]. A closed $N = 126$ shell configuration is assumed for the parent nucleus. Proton holes in $0h_{11}$, $1d_{3/2}$, and $2s_{1/2}$ orbits are taken into account for the shell-model calculations. Configurations with 2–4 and up to two holes are taken for $1d_{3/2}$ and $2s_{1/2}$ orbits, respectively. For the $0h_{11/2}$ orbit, $(n_h - 6)$–$(n_h - 4)$ (~ 12 in the case of $n_h = 17$) hole configurations are taken into account for $n_h \leqslant 17$. In the case of $n_h = 18$ ($Z = 64$), 10–12 hole configurations for the $0h_{11/2}$ orbit and an additional 0–2 hole configurations for the $1d_{5/2}$ orbit are considered. For neutrons, the $0h_{9/2}$, $1f_{5/2,7/2}$, $2p_{1/2,3/2}$, and $0i_{13/2}$ orbits outside the $N = 82$ core are taken as the model space, and in the β decays a neutron in these orbits changes into a proton whose orbit has holes. The FF transitions are induced by $\nu 0i_{13/2} \to \pi 0h_{11/2}$ and $\nu(fp) \to \pi(sd)$ transitions while the GT transition is dominantly induced by the $\nu 0h_{9/2} \to \pi 0h_{11/2}$ transition. In the β decays, important contributions come from transitions to low-lying states. The giant resonance region is energetically off the β-decay windows even for the very neutron-rich cases. Though the calculations have been carried out with restricted
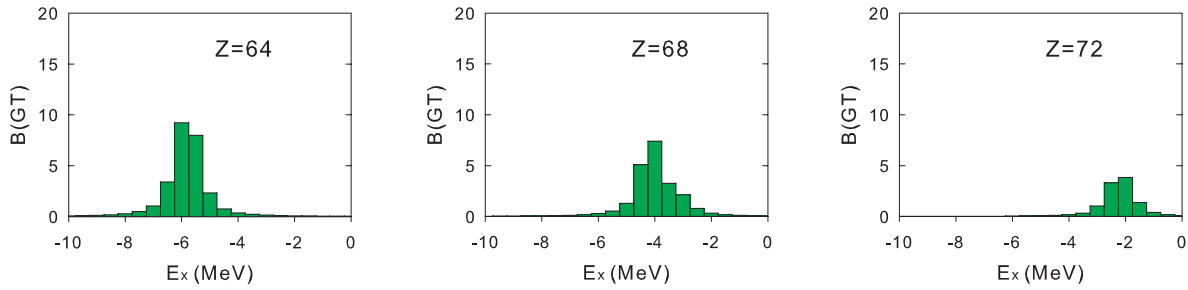
FIG. 1. (Color online) GT strengths for the isotone with $Z = 64$, 68, and 72 obtained by the shell-model calculation at energies from the parent state.

configurations, important states with low excitation energies are considered to be well described by the present shell-model calculations.

The GT transition strengths, $B(GT) = K_0$ [Eq. (2)], obtained by the shell-model calculations are shown in Fig. 1. Here, g_A is taken to be quenched by a factor of 0.7 [28,29], that is, $g_A = 0.7 \times g_A^{\text{free}}$ with $g_A^{\text{free}} = -1.26$. Energies denoted are those from the parent state. As the proton hole number increases, the energy difference between the parent state and the daughter states at the peak of the strength and the phase space for the transition becomes larger. Note that the transition strength is approximately proportional to the fifth power of the energy difference. The summed GT strength also becomes generally larger for more proton holes; the sum of the calculated $B(GT)$ values are 14.4, 14.6, 11.7, 8.5, and 5.6 for $Z = 64, 66, 68, 70$, and 72, respectively. Both of the effects lead to shorter half-lives for the isotones with larger proton hole number in the β decays.

We find that the most important contributions from the FF transitions come from the case of $J^\pi = 1^-$. We discuss spin-dipole strengths, which are important spin-dependent contributions in K_0 as well as the total shape factors averaged over electron energy. Calculated spin-dipole strengths

$$B(SD\lambda) = \frac{1}{2J_i + 1} |\langle f || r[Y^{(1)} \times \vec{\sigma}]^\lambda t_- || i \rangle|^2 \quad (7)$$

with $\lambda = 1$ are shown in Fig. 2 (upper figures). A general feature of the strength distributions is similar to the case of the GT transitions. The energy difference between the parent state and the daughter states at the peak of the strength as well as the sum of the strength get larger for nuclei with more proton holes. The summed $B(SD1)$ values are 55.5, 49.2, 48.4, 40.1, and 35.1 fm^2 for $Z = 64, 66, 68, 70$, and 72, respectively.

In the case of FF transitions, as the shape factor $C(w)$ depends on electron energy, it is more appropriate to discuss the averaged shape factor instead of K_0. Following Ref. [25], the averaged shape factor is defined as

$$\overline{C(w)} = f/f_0 \quad (8)$$

with

$$f_0 = \int_1^{w_0} F(Z, w) p w (w_0 - w)^2 dw, \quad (9)$$
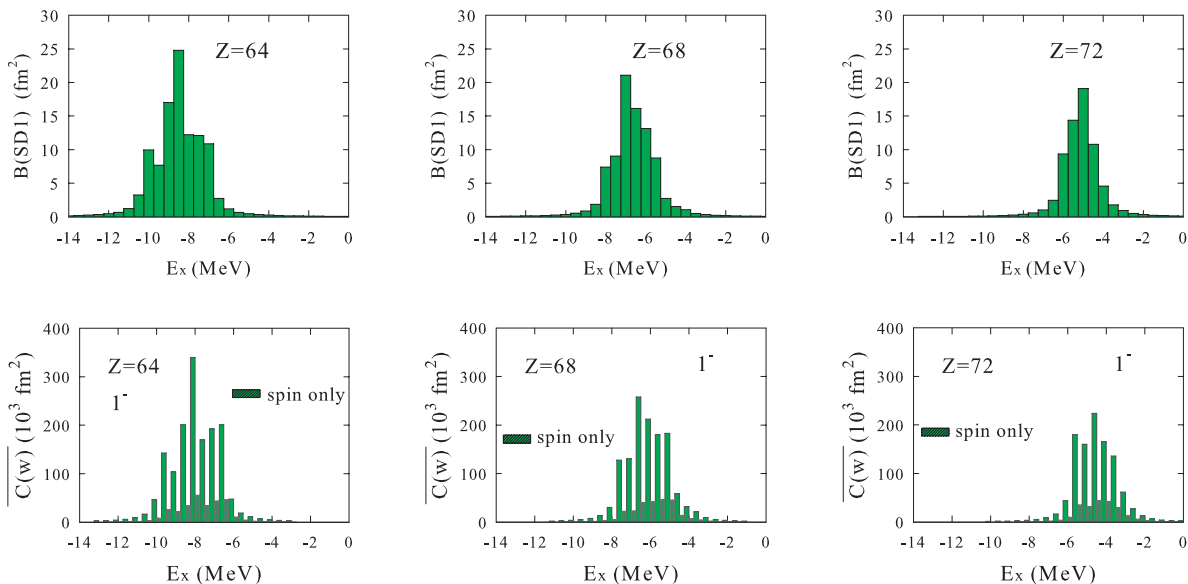

FIG. 2. (Color online) The same as in Fig. 1 for the spin-dipole strengths with $J^\pi = 1^-$ (upper figures) and the corresponding average shape factors (lower figures) for the isotones.

TABLE I. Calculated half-lives (in units of ms) for the β decays of $N = 126$ isotones obtained by shell-model calculations with the use of the quenching factor of $g_A/g_A^{\text{free}} = 0.7$ for 1^+, 1^-, and 2^- transitions. The enhancement factor of $\epsilon = 2.0$ is used for the matrix element M_0^T in 0^- transitions. Results for the GT transitions as well as those for both the GT and FF transitions are shown for $Z = 64-73$. Results for the case of the approximation, $\mu_1 = \lambda_2 = 1$, in the FF transitions are also shown.

Z	64	65	66	67	68	69	70	71	72	73
GT (ms)	5.76	7.69	11.26	17.46	29.31	54.77	102.49	223.26	504.79	1584.4
GT + FF (ms)	4.02	5.31	7.75	10.94	18.11	29.49	44.18	84.81	129.65	278.88
GT + FF ($\lambda_2 = 1$, $\mu_1 = 1$) (ms)	4.01	5.31	7.74	10.94	18.08	29.48	44.07	84.73	129.24	278.35

and for FF transitions

$$\overline{C(w)} = \frac{9195 \times 10^5}{f_0 t} \quad (\text{fm}^2). \qquad (10)$$

Averaged shape factors for 1^- transitions are shown in Fig. 2 (lower figures). Here the matrix elements are multiplied by the electron Compton wavelength so that they have a dimension of "fm." The transitions have components from the hadronic vector current also, that is, the contributions from the electric dipole ($E1$) transitions. We see from Fig. 2 that the the total contributions have similar strength distributions as those of the spin-dipole part, while the contributions from the spin independent part are large. The peak position of the transition strength in nuclei near $Z \sim 70$ is located at β-decay energies of about 6 MeV (4 MeV) for the 1^- (GT) transition, which is found to be similar to the case of the CQRPA calculation in Ref. [15].

B. Half-lives of the waiting-point nuclei

Decay rates and relevant matrix elements for the GT and FF transitions are evaluated [19] by including the quenching of the axial vector coupling constant: $g_A/g_A^{\text{free}} = 0.7$ is taken in the present study for both the GT and FF transitions except for the 0^- case. In relation to this, a similar order of quenching is found for the spin g factor, $g_s^{\text{eff}} = 0.64 g_s$, in the study of

spin-dipole $M2$ transitions in heavy nuclei [30]. We therefore assume the same quenching in the spin-dipole transitions for 1^- and 2^- cases as in the GT transitions.

As for the 0^- case, g_A in M_0^T ($\vec{\sigma} \cdot \vec{p}$ term from γ_5) is enhanced due to the meson exchange current effects [25]. The enhancement factor is taken to be $\epsilon = g_A/g_A^{\text{free}} = 2.0$ while it is taken to be 1.0 in M_0^S ($\vec{\sigma} \cdot \vec{r}$ term) following the analysis in Ref. [25], where $\epsilon = 2.01 \pm 0.05$ and 0.97 ± 0.06 are obtained for M_0^T and M_0^S, respectively, by fitting to the experimental β-decay data for $A = 205-212$.

Calculated half-lives for the β decays of the isotones are shown in Table I and Fig. 3(a). Calculated β-decay Q values obtained in the shell-model calculations are used. Calculated half-lives obtained with an approximation of using $\mu_1 = \lambda_2 = 1$ are also shown in Table I. This approximation changes the half-lives by only within 0.3%. (The effects on the FF transition rates are within 0.5%.) As the approximation proves to be quite accurate even for the present large Z cases, we adopt $\mu_1 = \lambda_2 = 1$ hereafter. The validity of this approximation is also pointed out in Ref. [25] for nonunique FF transitions.

Calculated half-lives obtained by the GT contributions only are found to be close to those in Refs. [10,16,31] within $\sim$10% except for $Z = 71$ and 73. In case of $Z = 71$ and 73, the half-lives obtained here are shorter by about $1.3-1.5$ than those in Refs. [10,16]. The shell-model interaction used here [17] is not the same as that in Refs. [10,16]. The half-lives become
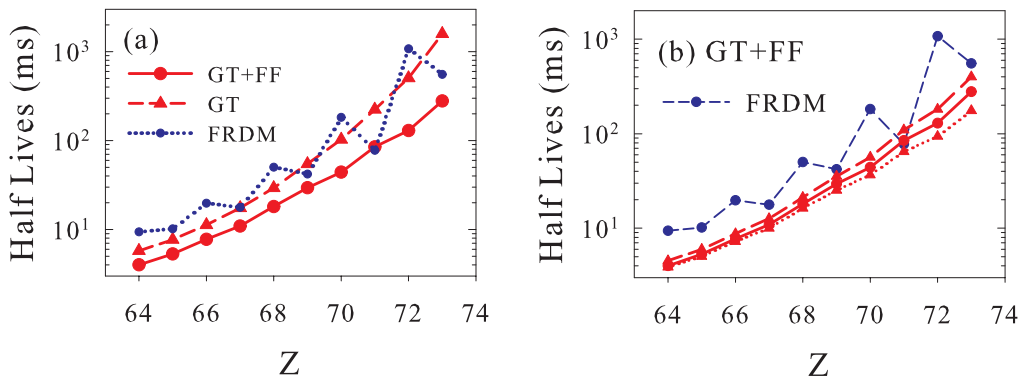

FIG. 3. (Color online) (a) Calculated half-lives for the $N = 126$ isotones. Results of the present shell-model calculations with GT and with GT + FF transitions are denoted by dashed and solid curves, respectively. The quenching factor of $g_A/g_A^{\text{free}} = 0.7$ is used for both the GT and FF transitions except for 0^- transitions (see text). Half-lives of Ref. [12] denoted as FRDM are shown by a dotted curve. (b) The same as in Fig. 3(a) for the shell-model calculations with contributions from both the GT and FF transitions. The solid curve and the curve denoted as FRDM are the same as in (a), while the long-dashed and dotted curves are obtained by using a different quenching factor of $g_A/g_A^{\text{free}} = 0.34$ with further quenching of $g_V/g_V^{\text{free}} = 0.67$. In case of the dotted curve, the Q values are increased by 1 MeV for the isotones in the FF transitions.

shorter for isotones with smaller Z as both the strength and the energy difference between initial and final states get larger. The FF transitions are found to be important to reduce the half-lives by $1.4-5.7$ times those given by the GT contributions only. Their contributions become more important compared to the GT ones for larger Z cases. The dominant contributions come from the 1^- transitions. The contributions from the 0^- transitions are about 10% of the total FF contributions; $7-8\%$ for $Z = 64-68$, $9-10\%$ for $Z = 69-71$, and 11% (13%) for $Z = 72$ (73). The reduction of the half-lives due to the inclusion of the FF transitions is not as large as that obtained in Ref. [15]. The half-lives obtained here are, however, short compared with the standard data of Ref. [12] except for $Z = 71$ usually employed in nucleosynthesis network calculations as shown in Fig. 3(a). The present half-lives of the shell-model calculations are shorter than those of the standard values by $2.3-8.3$ for even Z and by $1.4-2.0$ for odd Z (except for $Z = 71$), respectively. They increase monotonically as Z increases showing no odd-even staggering found in FRDM's. This is due to the absence of the odd-even staggering in the β-decay Q values in the shell-model calculations in contrast to the case of FRDM calculations.

The present half-lives are longer than those of Ref. [15] by about $1.1-1.3$ (1.5) for $Z = 64-67$ (68) and by twice for $Z = 69$ and 70, respectively. They are, on the other hand, short compared to the half-lives of Ref. [31], where similar CQRPA calculations have been done as in Ref. [15] but without energy dependent smearing of the GT and FF transition strengths. The present half-lives are shorter than those of Ref. [31] by about a factor of 1.5 for $Z = 69$, 70 and about by twice for $Z = 72$, 73, while they are close to each other for $Z = 64-68$ and 71. As the shell-model calculations include the spreading of the GT and FF transition strengths, it is reasonable that shorter half-lives are obtained in the present calculations.

We here consider other possible quenching factors for 1^- transitions. A large quenching of g_A and g_V for 1^- spin-dipole transitions was suggested by studies of FF β decays and related processes in the lead region [18,25,26]. In Ref. [26], effective quenching factors of $g_A/g_A^{\text{free}} \sim 0.47$ and $g_V/g_V^{\text{free}} \sim 0.64$ due to core polarization effects are obtained for 1^- transitions. In Ref. [18], two sets of quenching factors, $g_A/g_A^{\text{free}} = 0.34$, $g_V/g_V^{\text{free}} = 0.67$ and $g_A/g_A^{\text{free}} = 0.51$, $g_V/g_V^{\text{free}} = 0.30$, are obtained from the analysis of the FF transition, ^{205}Tl ($1/2^+$, g.s.) $\rightarrow$ ^{205}Pb ($1/2^-$).

We study FF β decays in nuclei with $Z = 78-80$ and $N = 126$, where experimental data are available for 0^- and 1^- transitions [32]. Calculated values of $\log f_0 t$ and $\sqrt{C(w)}$ (fm) for the FF β decays, ^{206}Hg $\rightarrow$ ^{206}Tl (0^-, 1^-) and ^{205}Au $\rightarrow$ ^{205}Hg ($1/2^-$, $3/2^-$, $5/2^-$), are given in Table II for the following sets of the quenching factors: $(g_A/g_A^{\text{free}}, g_V/g_V^{\text{free}}) =$ (a) (0.34, 0.67) [18], (b) (0.51, 0.30) [18], and (c) (0.47, 0.64) [26] for 1^- transitions. Experimental values [32] as well as the calculated values given in Ref. [25] for $Z = 80$ and cases for some other sets of quenching such as (0.34, 0.40) and (0.34, 0.94) are also given. In the case of 0^- transitions, the enhancement factor of $\epsilon = g_A/g_A^{\text{free}} = 1.45-2.0$ is adopted for the matrix element M_0^T. Values in parentheses in the table are for the case in which proton holes are restricted to $0h_{11/2}$, $1d_{3/2}$, and $2s_{1/2}$ orbits.

In the case of $Z = 80$, for the 0^- transition, calculated $\log f_0 t$ and $\sqrt{C(w)}$ values for $\epsilon = 2.0$ are close to those of Ref. [25] and become closer to the experimental values for $\epsilon = 1.8$. For the 1^- transition, the calculated $\log f_0 t$ values for the sets (a), (b), and (c) are smaller than those of Ref. [25] by 0.17, 0.02, and 0.26, respectively. They get closer to the observed values if a set with more quenching for g_V, (0.34, 0.40), is used.

In the case of $Z = 79$, transitions to the $1/2_1^-$ and $5/2_1^-$ states in ^{205}Hg are dominantly induced by 1^- transitions, while the transition to the $3/2_1^-$ state is a mixture of 0^- and 1^- transitions. For the 1^- transition to the $1/2_1^-$ (g.s.) state, the three sets of the quenching give larger (smaller) $\log f_0 t$ [$\sqrt{C(w)}$] values than the experimental ones. A set with smaller quenching for g_V, (0.34, 0.94), gives the values close to the experiment. For the transition to the $3/2_1^-$ state ($E_x = 0.4675$ MeV), the 0^- transition proceeds too fast for $\epsilon = 2.0$. When an enhancement factor of $\epsilon = 1.45$ is used, the three sets of the quenching for the 1^- transitions can give $\log f_0 t$ and $\sqrt{C(w)}$ values close to the experimental ones. The set used for the $1/2_1^-$ case, (0.34, 0.94), works also in this transition. As for the $5/2_1^-$ state, any of the three sets of the quenching for the 1^- transition give transitions too fast compared to the experiment. In this case, an exceptionally large quenching, (0.10, 0.15), is necessary to explain the experiment.

Although the spins of the excited states of ^{205}Hg at $E_x = 1.2806$ MeV and $E_x = 1.4472$ MeV are not determined yet, the present analysis suggests that the state at $E_x = 1.2806$ MeV is $3/2^-$ or $5/2^-$ and the state at $E_x = 1.4472$ MeV is $1/2^-$ (see Table II). Other possibilities, that is, $1/2^-$ ($3/2^-$ and $5/2^-$) for the state at $E_x = 1.2806$ MeV (1.4472 MeV) can be excluded.

In the case of $Z = 78$, the half-life for the transition ^{204}Pt (0^+) $\rightarrow$ ^{204}Au has been obtained by measuring two γ decays in ^{204}Au [32]. The averaged experimental half-life is 10.3 s. Here, the half-life is calculated by taking into account the FF 0^- and 1^- transitions. The enhancement factor of $\epsilon = 2.0$ is used for the 0^- transition. The half-lives obtained with the three sets of the quenching for the 1^- transitions are given in Table III. The calculated half-lives are longer than the observed one by about $2-3$. The values become close to the observed one for the cases without quenching for g_V (see Table III). The present analysis suggests smaller quenching for g_V for $Z = 78$.

The present analysis for $Z = 78-80$ suggests a large quenching for g_A. A large quenching for g_V is not necessarily needed for $Z = 78$ and for most cases of $Z = 79$. We study dependence of the calculated half-lives on the quenching of g_A and g_V. Half-lives obtained with the set (a) for the 1^- transitions are shown in Fig. 3(b). The enhancement factor ϵ for the 0^- transitions is not changed: $\epsilon = 2.0$. The half-lives get longer but still remain shorter than those of Ref. [12] except for $Z = 71$. They become close to the values of Ref. [31].

Although the experimental Q values are used for the analysis of the β decays for $Z = 78-80$, the present shell-model calculations give smaller Q values compared to the experimental ones. The differences are 1.3, 1.6, and 0.9 MeV for $Z = 80$, 79, and 78, respectively. As there are no experimental

TABLE II. Values of $\log f_0 t$ and $\sqrt{C(w)}$ for FF transitions in nuclei with $Z = 79, 80$ and $N = 126$. Calculated values obtained by using quenching factors of $(g_A/g_A^{\text{free}}, g_V/g_V^{\text{free}})$ for 1^- transitions and enhancement factor ϵ for 0^- transitions as well as experimental values [32] are shown. Values of Ref. [25] are also shown for $Z = 80$. Values of $\log f_0 t$ and $\sqrt{C(w)}$ in the parentheses are for the case in which proton holes are restricted to $0h_{11/2}$, $1d_{5/2}$, and $2s_{1/2}$ orbits.

Transitions		Values of g_A and g_V		$\log f_0 t$	$\sqrt{C(w)}$ (fm)
Initial	Final	ϵ for 0^-	$(g_A/g_A^{\text{free}}, g_V/g_V^{\text{free}})$ for 1^-		
^{206}Hg (0^+)	^{206}Tl $(0^-$ g.s.$)$	2.0		5.199(5.087)	76.3(86.8)
		1.8		5.432(5.320)	58.3(66.3)
		Ref. [25]		5.173	78.6
	Expt. [32]			5.41	59.8
^{206}Hg (0^+)	^{206}Tl $(1^-, 0.3049$ MeV$)$		(a) (0.34, 0.67)	5.017(4.929)	94.0(104.1)
			(b) (0.51, 0.30)	5.157(5.127)	80.0(82.9)
			(c) (0.47, 0.64)	4.921(4.832)	105.0(116.4)
			(0.34, 0.40)	5.267(5.178)	70.5(78.2)
			Ref. [25]	5.181	77.9
	Expt. [32]			5.24	72.7
^{205}Au $(3/2^+)$	^{205}Hg $(1/2_1^-)$		(a) (0.34, 0.67)	6.197(6.116)	24.2(26.5)
			(b) (0.51, 0.30)	8.171(7.834)	2.49(3.67)
			(c) (0.47, 0.64)	6.412(6.326)	18.9(20.8)
			(0.34, 0.94)	5.793(5.726)	38.7(41.6)
	Expt. [32]			5.79	38.6
^{205}Au $(3/2^+)$	^{205}Hg $(3/2_1^-, 0.4675$ MeV$)$				
	0^-	2.0		5.674(5.541)	44.1(51.5)
		1.45		6.832(6.699)	11.6(13.6)
	$0^- + 1^-$	1.45	(a) (0.34, 0.67)	6.502(6.247)	17.0(22.8)
		1.45	(b) (0.51, 0.30)	6.000(5.870)	30.3(35.2)
		1.45	(c) (0.47, 0.64)	6.266(6.073)	22.3(27.9)
		1.45	(0.34, 0.94)	6.425(6.173)	18.6(24.9)
	Expt. [32]			6.43	18.5
^{205}Au $(3/2^+)$	^{205}Hg $(5/2_1^-, 0.3792$ MeV$)$		(a) (0.34, 0.67)	5.108(5.006)	84.7(95.2)
			(b) (0.51, 0.30)	5.409(5.308)	59.9(67.3)
			(c) (0.47, 0.64)	5.057(4.956)	89.8(100.9)
			(0.10, 0.15)	6.343(6.242)	20.4(23.0)
	Expt. [32]			6.37	19.8
^{205}Au $(3/2^+)$	^{205}Hg $(3/2_2^-, 1.2806$ MeV$)$				
	$0^- + 1^-$	1.5	(a) (0.34, 0.67)	5.497(5.457)	54.1(56.7)
		1.5	(b) (0.51, 0.30)	5.556(5.454)	50.6(56.8)
		1.5	(c) (0.47, 0.64)	5.433(5.413)	58.3(59.6)
		1.5	(0.34, 0.94)	5.364(5.374)	63.0(62.4)
	Expt. [32]			5.51	53.3
^{205}Au $(3/2^+)$	^{205}Hg $(5/2_2^-, 1.2806$ MeV$)$		(a) (0.34, 0.67)	5.397(5.807)	60.7(37.9)
			(b) (0.51, 0.30)	5.646(6.064)	45.6(28.2)
			(c) (0.47, 0.64)	5.333(5.746)	65.4(40.6)
			(0.34, 0.94)	5.176(5.584)	78.3(48.9)
	Expt. [32]			5.51	53.3
^{205}Au $(3/2^+)$	^{205}Hg $(1/2_2^-, 1.4472$ MeV$)$		(a) (0.34, 0.67)	6.632(6.163)	14.7(25.1)
			(b) (0.51, 0.30)	7.191(7.956)	7.7(3.2)
			(c) (0.47, 0.64)	6.708(6.386)	13.4(19.4)
			(0.34, 0.94)	6.300(5.767)	21.5(39.7)
	Expt. [32]			6.29	21.7

information on the Q values for $Z = 64$–73, we used the calculated Q values. They are small compared to the mass differences between the parent and daughter nuclei in Ref. [12] by about 2 MeV (3 MeV) for even (odd) Z nuclei. Now, we study the dependence of the half-lives on the Q values of the transitions. Calculated half-lives are shown in Fig. 3(b) for

the case in which the Q values obtained by the shell-model calculations are increased by 1 MeV for the isotones with $Z = 64$–73. The effects of the change of the Q values, which results in the enhancement of the phase-space volumes, are found to be large. The half-lives get shorter than the case in Fig. 3(a) with the quenching, (0.7, 1.0), but they do not become

TABLE III. Half-life for the β decay of ^{204}Pt. Calculated values obtained by using quenching factors of $(g_A/g_A^{\text{free}}, g_V/g_V^{\text{free}})$ for 1^- transitions and enhancement factor ϵ for 0^- transitions as well as experimental value [32] are shown. Values of the half-life in the parentheses are for the case in which proton holes are restricted to $0h_{11/2}$, $1d_{5/2}$, and $2s_{1/2}$ orbits.

Transitions		Values of g_A and g_V		Half-life (s)
Initial	Final	ϵ for 0^-	$(g_A/g_A^{\text{free}}, g_V/g_V^{\text{free}})$ for 1^-	
^{204}Pt (0^+)	^{204}Au (0^-)	2.0		65.1(62.0)
^{204}Pt (0^+)	^{204}Au $(0^- + 1^-)$	2.0	(a) (0.34, 0.67)	22.8(18.6)
		2.0	(b) (0.51, 0.30)	31.8(26.9)
		2.0	(c) (0.47, 0.64)	21.1(17.1)
		2.0	(0.7, 1.0)	10.9(8.6)
		2.0	(0.34, 1.0)	14.4(11.3)
		2.0	(0.51, 1.0)	12.7(10.0)
	Expt. [32]			10.3 ± 1.4

as short as those of Ref. [15]. They are still longer than those of Ref. [15] by about 30% for $Z = 66$–68 and 50% (60%) for $Z = 69$ (70). It is quite important to obtain experimental information on the masses of waiting point nuclei and their daughters.

III. *R*-PROCESS NUCLEOSYNTHESIS

We discuss possible effects of the short half-lives of the waiting point nuclei at $N = 126$ obtained in the preceding section on the r-process nucleosynthesis. The dependence of the abundances of the elements around mass number $A \sim 195$ on the half-lives of the nuclei is investigated for various astrophysical conditions. We use an analytic model for neutrino-driven winds [33] for the time evolution of thermal profiles. The wind solutions that pass the sonic points are adopted. We take into account the relation of the neutrino luminosity L_ν and the mean neutrino energy to the entropy

TABLE IV. The mass shift at the third peak of the element abundance in the r process defined by Eq. (11) as well as the peak position for the case of the modified half-lives are shown for several astrophysical conditions. The ratio (R) of the height of the second peak over that of the third peak is also given. For each astrophysical condition, the first row corresponds to the case of the quenching of $(g_A/g_A^{\text{free}}, g_V/g_V^{\text{free}}) = (0.70, 0.0)$, while the second and third rows correspond to the case of (a) (0.34, 0.67) for 1^- transitions. The Q value is increased by 1 MeV for the third row [denoted as (a)*].

$L_{\nu,51}$	S/k	$\dot{M}$ $(M_\odot$ s$^{-1})$	f_t	τ (ms)	Ratio R	$\langle A \rangle_{\text{Mod}}$	ΔA
0.5	133.4	2.34×10^{-6}	0.06	5.60	3.45	196.972	1.101
					(a) 3.21	196.684	0.813
					(a)* 3.84	197.218	1.347
1.0	118.9	7.43×10^{-6}	0.08	4.04	4.23	197.118	1.058
					(a) 3.89	196.837	0.777
					(a)* 4.75	197.359	1.299
2.0	105.9	2.36×10^{-5}	0.10	2.90	4.77	197.234	1.008
					(a) 4.35	196.965	0.739
					(a)* 5.03	197.466	1.240
5.0	90.91	1.08×10^{-4}	0.11	1.78	3.80	197.313	0.949
					(a) 3.52	197.066	0.702
					(a)* 3.94	197.523	1.159

per baryon S/k and the mass ejection rate $\dot{M}$ of the winds in accordance with [34]. The neutrino energy spectra are assumed to obey Fermi distributions with zero chemical potentials. The temperatures of ν_e, $\bar{\nu}_e$, and $\nu_x = \nu_{\mu,\tau}$ and $\bar{\nu}_{\mu,\tau}$ are set to be $(T_{\nu_e}, T_{\bar{\nu}_e}, T_{\nu_x}) = (3.2, 5, 6$ MeV) [35]. The luminosity of each flavor of neutrinos is equipartitioned and is taken to be $L_\nu = (0.5-5.0) \times 10^{51}$ erg s^{-1}. The neutrino luminosity, entropy per baryon, and mass ejection rate of each wind model are listed in Table IV.

We calculate r-process nucleosynthesis using a reaction network consisting of 3517 species of nuclei. The initial electron to baryon ratio is taken to be $Y_e = 0.40$. Neutrino processes on nucleon and ^{4}He are included in the network calculations. Charged current reactions, $n(\nu_e, e^-)p$, $p(\bar{\nu}_e, e^+)n$, ^{4}He$(\nu_e, e^- p)^3$He, and ^{4}He$(\bar{\nu}_e, e^+ n)^3$H give dominant contributions. Besides them, charged current reactions, ^{4}He$(\nu_e, e^- pp)^2$H, ^{4}He$(\bar{\nu}_e, e^+ nn)^2$H, and neutral current reactions, ^{4}He$(\nu, \nu'n)^3$He, ^{4}He$(\nu, \nu'p)^3$H, ^{4}He$(\nu, \nu'd)^2$H, ^{4}He$(\nu, \nu'nnp)^1$H, and those induced by $\bar{\nu}$'s, are included. Cross sections of Ref. [36] obtained by the WBP Hamiltonian [37] are used. The cross sections of n and p are adopted from [38]. The neutrino processes suppress the production of the elements around the third peak in the r process as neutrons are changed into protons, which results in the increase of Y_e, and the production of seed elements is enhanced through the neutrino-induced breakup of ^{4}He [9]. We artificially shorten the time scale of the explosion by a constant factor f_t in order to proceed the r process to the synthesis of the third peak elements because it was found that the shorter expansion time scale tends to decrease the roles of neutrino interactions and keep low Y_e in favor of the r process [2]. We set the final temperature of the winds to be $T_f = 8 \times 10^8$ K. The duration time τ where the temperature decreases from 5×10^9 K to 2×10^9 K is $\tau = (1.8-5.6)$ ms. The multiplying factor f_t and the duration time τ for the r-process calculation are also shown in Table IV.

The abundance of the elements obtained by using the present short half-lives in the r-process element network are compared with those obtained with the use of the standard data of Ref. [12]. We show in Fig. 4 a case in which the ratio of the height of the third peak over that of the second peak in the r process is close to the solar abundance ratio, 3−4. Parameters chosen are $L_{\nu,51} = 0.5$ where $L_{\nu,51} = L_\nu/(10^{51}$erg s$^{-1})$,
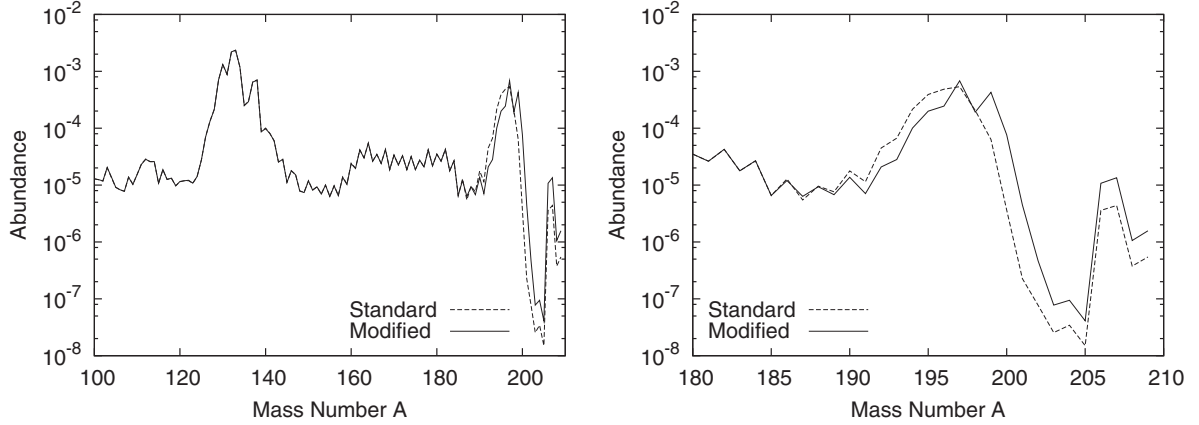
FIG. 4. The abundances of elements in the r-process nucleosynthesis obtained by using the present β-decay half-lives for the $N = 126$ isotones (denoted as "modified") and standard half-lives of Ref. [12] (denoted as "standard"). The quenching factor of $g_A/g_A^{\rm free} = 0.7$ ($g_V/g_V^{\rm free} = 1.0$) is used both for the GT and FF (1^- and 2^-) transitions. The right figure displays the same result in the restricted range of $A \geqslant 180$.

$S/k = 133$ and $\tau = 5.6$ ms. Here, the half-lives obtained for the case with the quenching of $g_A/g_A^{\rm free} = 0.7$ ($g_V/g_V^{\rm free} = 1$) for 1^- transitions are used. Other inputs except for the half-lives are not changed. We show in Fig. 5 the calculated results for the case of a different set of the quenching factors for 1^- transitions, $(g_A/g_A^{\rm free}, g_V/g_V^{\rm free}) = (0.34, 0.67)$. A case with Q values increased by 1 MeV is also shown. We find a slight shift of the third peak of the element abundances toward higher mass region. This shows more rapid buildup of the r-process elements caused by the shorter half-lives of the waiting point nuclei. The isotones with higher Z accumulate more abundantly at the freezing time of the neutron-capture flow, which by successive β decays naturally results in larger abundances of the elements at higher mass region.

When the decrease of the temperature becomes slower or the entropy of the system is larger, the magnitude of the shift of the peak gets larger. The shift of the mass number at the third peak region is defined by

$$\Delta A = \langle A \rangle_{\rm Mod} - \langle A \rangle_{\rm STD} \quad \langle A \rangle = \frac{\sum_A A \cdot Y(A)}{\sum_A Y(A)}, \quad (11)$$

where $Y(A)$ is the abundance of the element with mass number A and the summation is taken over $189 \leqslant A \leqslant 203$. "Mod" and "STD" refer to the cases of modified half-lives and standard ones, respectively. The mass shifts at the third peak of the r process are shown in Table IV for several different values of $L_{\nu,51}$, S/k, and τ. Here, the condition is being kept so that the ratio of the height of the third peak over that of the second peak is close to the solar abundances ratio. We see from Table IV that the mass shift ΔA is about unity in all cases. Dependence on the astrophysical condition is found to be small. Dependence on the difference of the quenching factors is also as small as $25-30\%$. The decrease of the mass shift due to larger quenchings is recovered or even reversed to an increase by the change of the Q values. We also find that the mass shift at the second peak, where the average is taken over $124 \leqslant A \leqslant 136$, is quite small; $\Delta A = -0.006 - +0.002$. We thus emphasize that the shift of the third peak of element abundance toward higher mass region by about unity is a common phenomenon in the present astrophysical conditions. When half-lives of the $N = 82$ isotones are changed to the values obtained by shell-model calculations [11], effects on
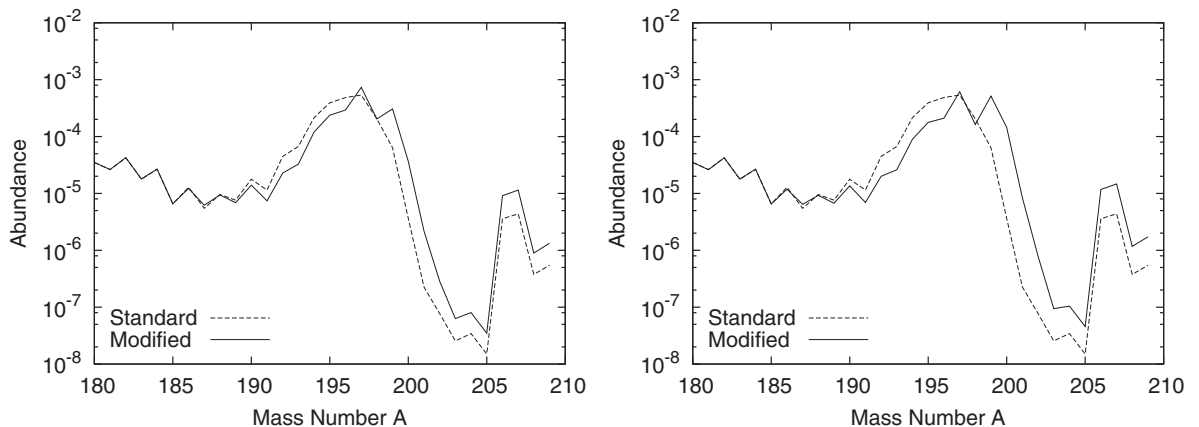

FIG. 5. The same as in Fig. 4 at $A \geqslant 180$ for the quenching factors of $(g_A/g_A^{\rm free}, g_V/g_V^{\rm free}) = (0.34, 0.67)$ for the 1^- transitions. The figure on the right side includes the effect of the increase of the Q values.

the shift of the third peak is found to be quite small. The mass shift ΔA decreases only by 6% while the mass shift at the second peak is $\Delta A = 0.26-0.28$. The magnitude of the shift at the third peak is rather modest, but it is a robust effect and is of the same order as that caused by variations of mass formulas. As we see from Table IV, the position of the third peak of the solar abundance, $A \sim 195$, is not necessarily reproduced by the present calculations. However, we should note that the third peak region can be affected by various effects besides the half-lives of the β decays as we pointed out. Neutron-star merger and γ-ray bursts are considered to be possible alternative r-process sites [4,5]. The assignment of the site of the r process including those besides the supernova explosions is an important and interesting subject to be explored further in the future.

IV. SUMMARY

In summary, we have evaluated half-lives of the β decays of $N = 126$ isotones taking into account both the GT and FF transitions. The half-lives have been found to be reduced by including the FF transitions. The effects of the short half-lives obtained here on the nucleosynthesis of the r process are investigated. The third peak of the abundance of the elements in the r process has been found to be shifted toward higher mass region. Although the magnitude of the shift is rather modest, it is found to be a robust effect independent of the present astrophysical conditions for the r process as well as the quenching factors of g_A and g_V adopted in the shell-model calculations. The results obtained here might be improved quantitatively by overcoming the limitations in the present structure calculations such as configuration space. Improvements of various nuclear properties for the input for the nucleosynthesis network of the r process in addition to the β-decay half-lives, especially the masses of nuclei at and around the waiting points, are important issues to be made in future studies.

[1] E. M. Burbidge, G. R. Burbidge, W. A. Fowler, and F. Hoyle, Rev. Mod. Phys. **29**, 547 (1957); J. J. Cowan, F.-K. Thielemann, and J. W. Truran, Phys. Rep. **208**, 267 (1991) ; K.-L. Kratz, J. Bitouzet, F.-K. Thielemann, P. Möller, and B. Pfeiffer, Astrophys. J. **403**, 216 (1993).

[2] B. S. Meyer, G. Mathews, W. M. Howard, S. E. Woosley, and R. D. Hoffman, Astrophys. J. **393**, 656 (1992); S. E. Woosley, J. R. Wilson, G. J. Mathews, R. D. Hoffman, and B. S. Meyer, *ibid.* **433**, 229 (1994); K. Otsuki, H. Tagoshi, T. Kajino, and S. Wanajo, *ibid.* **533**, 424 (2000); S. Wanajo and Y. Ishimaru, Nucl. Phys. A **777**, 676 (2006).

[3] S. Wanajo, M. Tamamura, N. Itoh, K. Nomoto, Y. Ishimaru, T. C. Beers, and S. Nozawa, Astrophys. J. **593**, 968 (2003).

[4] C. Freiburghaus, S. Rosswog, and F.-K. Thielemann, Astrophys. J. **525**, L121 (1999).

[5] S. Fujimoto, M. Hashimoto, K. Kotake, and S. Yamada, Astrophys. J. **656**, 382 (2007); R. Surman, G. C. McLaughlin, M. Ruffert, H.-Th. Janka, and W. R. Hix, Astrophys. J. **679**, L117 (2008).

[6] S. Honda, W. Aoki, T. Kajino, H. Ando, T. C. Beers, H. Izumiura, K. Sadakane, and M. Takada-Hidai, Astrophys. J. **607**, 474 (2004).

[7] S. Wanajo, S. Goriely, M. Samyn, and N. Itoh, Astrophys. J. **606**, 1057 (2004).

[8] M. Terasawa, K. Sumiyoshi, T. Kajino, G. J. Mathews, and I. Tanihata, Astrophys. J. **562**, 470 (2001); T. Sasaqui, T. Kajino, G. Mathews, K. Otsuki, and T. Nakamura, *ibid.* **634**, 1173 (2005).

[9] B. S. Meyer, G. C. Mclaughlin, and G. M. Fuller, Phys. Rev. C **58**, 3696 (1998); M. Terasawa, K.-H. Langanke, T. Kajino, and G. Mathews, Astrophys. J. **609**, 470 (2004).

[10] K. Langanke and G. Martínez-Pinedo, Rev. Mod. Phys. **75**, 818 (2003); H. Grawe, K. Langanke, and G. Martínez-Pinedo, Rep. Prog. Phys. **70**, 1525 (2007).

[11] G. Martínez-Pinedo and K. Langanke, Phys. Rev. Lett. **83**, 4502 (1999).

[12] P. Möller, J. R. Nix, and K.-L. Kratz, At. Data Nucl. Data Tables **66**, 131 (1997); P. Möller, B. Pfeiffer, and K.-L. Kratz, Phys. Rev. C **67**, 055802 (2003).

[13] I. N. Borzov and S. Goriely, Phys. Rev. C **62**, 035501 (2000).

[14] J. Engel, M. Bender, J. Dobaczewski, W. Nazarewicz, and R. Surman, Phys. Rev. C **60**, 014302 (1999).

[15] I. N. Borzov, Phys. Rev. C **67**, 025802 (2003).

[16] G. Martínez-Pinedo, Nucl. Phys. A **688**, 357 (2001).

[17] S. J. Steer *et al.*, Phys. Rev. C **78**, 061302 (2008).

[18] L. Rydström, J. Blomqvist, R. J. Liotta, and C. Pomar, Nucl. Phys. A **512**, 217 (1990).

[19] E. K. Warburton, J. A. Becker, B. A. Brown, and D. J. Millener, Ann. Phys. **187**, 471 (1988); H. Behrens and W. Bühring, Nucl. Phys. A **162**, 111 (1971).

[20] H. Schopper, *Weak Interactions and Nuclear Beta Decays* (North-Holland, Amsterdam, 1966).

[21] I. S. Towner and J. C. Hardy, Nucl. Phys. A **179**, 489 (1972).

[22] B. A. Brown, C. R. Bronk, and P. E. Hodgson, J. Phys. G **10**, 1683 (1984).

[23] H. Behrens and J. Jänecke, *Numerical Tables for Beta-Decay and Electron Capture*, Landolt-Börnstein, New Series, Group I, Vol. 4, Table II (Springer-Verlag, Berlin, 1969).

[24] A. Bohr and B. R. Mottelson, *Nuclear Structure* (Benjamin, New York, 1969), Vol. I, p. 413.

[25] E. K. Warburton, Phys. Rev. C **44**, 233 (1991).

[26] E. K. Warburton, Phys. Rev. C **42**, 2479 (1990).

[27] OXBASH, B. A. Brown, A. Etchegoyen, and W. D. M. Rae, MSU Cyclotron Laboratory Report No. 524, 1986.

[28] C. Gaarde, in *Proceedings of the Niels Bohr Centennial Conference*, edited by R. Broglia, G. Hagemann, and B. Herskind (North-Holland, Amsterdam, 1985), p. 449.

[29] E. Caurier, G. Martínez-Pinedo, F. Nowacki, A. Poves, and A. P. Zuker, Rev. Mod. Phys. **77**, 427 (2005).

[30] P. von Neumann-Cosel, F. Neumeyer, S. Nishizaki, V. Yu. Ponomarev, C. Rangacharyulu, B. Reitz, A. Richter, G. Schrieder, D. I. Sober, T. Waindzoch, and J. Wambach, Phys. Rev. Lett. **82**, 1105 (1999).

[31] T. Kurtukian *et al.*, arXiv:0711.0101.

[32] National Nuclear Data Center on-line retrieval system [http://www.nndc.bnl.gov].

[33] K. Takahashi and H.-Th. Janka, in *Origin of Matter and Evolution of Galaxies*, edited by T. Kajino, S. Kubono, and Y. Yoshii (World Scientific, Singapore, 1997), p. 213.

[34] Y.-Z. Qian and S. E. Woosley, Astrophys. J. **471**, 331 (1996).

[35] T. Yoshida, M. Terasawa, T. Kajino, and K. Sumiyoshi, Astrophys. J. **600**, 204 (2004).

[36] T. Suzuki, S. Chiba, T. Yoshida, T. Kajino, and T. Otsuka, Phys. Rev. C **74**, 034307(R) (2006); T. Yoshida, T. Suzuki, S. Chiba, T. Kajino, H. Yokomakura, K. Kimura, A. Takamura, and D. H. Hartmann, Astrophys. J. **686**, 448 (2008).

[37] E. K. Warburton and B. A. Brown, Phys. Rev. C **46**, 923 (1992).

[38] C. J. Horowitz, Phys. Rev. D **65**, 043001 (2002).